High-resolution optical spectroscopy of the yellow hypergiant V1302 Aql (=IRC+10420) in 2001–2014

By: V.G. Klochkova, E.L. Chentsov, A.S. Miroshnichenko, V.E. Panchuk, M. V. Yushkin

Klochkova, V.G., Chentsov, E.L., Miroshnichenko, A.S., Panchuk, V.E., & Yushkin, M.V. (2016) High-resolution optical spectroscopy of the yellow hypergiant V1302 Aql (=IRC+10420) in 2001–2014, *Monthly Notices of the Royal Astronomical Society*, 459(4), 4183–4190. DOI: 10.1093/mnras/stw902

Abstract:

We present the results of a study of spectral features and the velocity field in the atmosphere and circumstellar envelope of the yellow hypergiant V1302 Aql, the optical counterpart of the IR source IRC+10420, based on high-resolution optical spectroscopic observations in 2001–2014. We measured heliocentric radial velocities of the following types of lines: forbidden and permitted pure emission, absorption and emission components of lines of ions, pure absorption (e.g. He I, Si II) and interstellar components of the Na I D lines, K Iand diffuse interstellar bands (DIBs). Pure absorption and forbidden and permitted pure emission, which have heliocentric radial velocities V_r = 63.7 ± 0.3, 65.2 ± 0.3 and 62.0 ± 0.4 km s^{-1}, respectively, are slightly redshifted relative to the systemic radial velocity (V_{sys} ∼ 60 km s^{-1}). The positions of the absorption components of the lines with inverse P Cyg profiles are redshifted by ∼20 km s^{-1}, suggesting that clumps falling on to the star have been stable over all observing dates. The average heliocentric radial velocity of the DIBs is V_r(DIB) = 4.6 ± 0.2 km s^{-1}. A Hα line profile with the red peak slightly stronger than the blue one was observed only once, on 2007 November 24. Comparison of pure absorption lines observed in 2001–2014 with those in earlier data does not show noticeable variations. The kinematic picture in the atmosphere was stable for observations during 2001–2014. Our results as a whole let us conclude that the hypergiant has reached a phase of slowing down (or termination) of effective temperature growth and is currently located near the high-temperature boundary of the Yellow Void in the Hertszprung–Russell diagram.

Keywords: techniques: spectroscopic | stars: individual: V1302 Aql | stars: massive | supergiants

***Note: Full text of article below

Monthly Notices
of the
ROYAL ASTRONOMICAL SOCIETY

MNRAS **459,** 4183–4190 (2016)
Advance Access publication 2016 April 20

doi:10.1093/mnras/stw902

High-resolution optical spectroscopy of the yellow hypergiant V1302 Aql (=IRC+10420) in 2001–2014

V. G. Klochkova,[1⋆] E. L. Chentsov,[1⋆] A. S. Miroshnichenko,[2] V. E. Panchuk[1] and M. V. Yushkin[1]

[1] *Special Astrophysical Observatory of the Russian Academy of Sciences, 369167 Nizhnij Arkhyz, Russia*
[2] *Department of Physics and Astronomy, University of North Carolina at Greensboro, Greensboro, NC 27402–6170, USA*

Accepted 2016 April 14. Received 2016 April 14; in original form 2016 January 19

ABSTRACT

We present the results of a study of spectral features and the velocity field in the atmosphere and circumstellar envelope of the yellow hypergiant V1302 Aql, the optical counterpart of the IR source IRC+10420, based on high-resolution optical spectroscopic observations in 2001–2014. We measured heliocentric radial velocities of the following types of lines: forbidden and permitted pure emission, absorption and emission components of lines of ions, pure absorption (e.g. He I, Si II) and interstellar components of the Na I D lines, K I and diffuse interstellar bands (DIBs). Pure absorption and forbidden and permitted pure emission, which have heliocentric radial velocities $V_r = 63.7 \pm 0.3$, 65.2 ± 0.3 and 62.0 ± 0.4 km s^{-1}, respectively, are slightly redshifted relative to the systemic radial velocity ($V_{sys} \sim 60$ km s^{-1}). The positions of the absorption components of the lines with inverse P Cyg profiles are redshifted by ∼20 km s^{-1}, suggesting that clumps falling on to the star have been stable over all observing dates. The average heliocentric radial velocity of the DIBs is V_r(DIB) $= 4.6 \pm 0.2$ km s^{-1}. A Hα line profile with the red peak slightly stronger than the blue one was observed only once, on 2007 November 24. Comparison of pure absorption lines observed in 2001–2014 with those in earlier data does not show noticeable variations. The kinematic picture in the atmosphere was stable for observations during 2001–2014. Our results as a whole let us conclude that the hypergiant has reached a phase of slowing down (or termination) of effective temperature growth and is currently located near the high-temperature boundary of the Yellow Void in the Hertszprung–Russell diagram.

Key words: techniques: spectroscopic – stars: individual: V1302 Aql – stars: massive – supergiants.

1 INTRODUCTION

The evolutionary status of the very luminous star V1302 Aql, the optical counterpart of the IR source IRC+10420, has been unclear. The variety in its properties allowed us to classify it as either a protoplanetary nebula (PPN: Hrivnak, Kwok & Volk 1989) or a very massive star that has passed through the red supergiant phase. PPNe are currently thought to be low-mass peculiar supergiants with strong IR excesses in a short-term transition from the asymptotic giant branch to the planetary nebula (PN) stage. They are descendants of intermediate-mass stars (initial masses 1–8 $M_\odot$) that have passed through several evolutionary stages, including switching of energy sources and stages with typical mass-loss rates up to 10^{-5} $M_\odot$ yr^{-1} and even up to 10^{-4} $M_\odot$ yr^{-1}. As a result, a PPN is a low-mass degenerate C–O core surrounded by a tenuous and usually asymmetric envelope. As the core contracts, its effective temperature (T_{eff}) rises and the star moves blueward in the Hertszprung–Russell diagram (hereafter HRD). This stage may last until T_{eff} reaches ∼30 000 K, when ionization of the circumstellar envelope begins. At this time, the object is observed as a PN after hydrogen recombination lines and forbidden lines of light elements show up in its spectrum. Luminosity of low-mass supergiants at the PPN stage may reach log $L/L_\odot \sim 4.5$ (Blöcker 1995).

Yellow supergiants are significantly different from PPNe, although a number of properties (high luminosity, spectral features, presence of circumstellar envelopes) are similar in these two classes of object. Predecessors of the former are massive (initial mass ≥20 $M_\odot$) and the most luminous stars, which lose a significant part of their mass after leaving the main sequence, become red supergiants and later proceed to yellow supergiants. A typical luminosity of a yellow supergiant is log $L/L_\odot \sim 5.3$–5.9 (Jones, Humphreys & Gehrz 1993). These objects are located near the Eddington limit in an instability region that contains hypergiants of spectral types from

⋆ E-mail: valenta@sao.ru (VGK); echen@sao.ru (ELC)

A–M (de Jager 1998; de Jager et al. 2001). Wolf–Rayet stars and luminous blue variables may be their descendants (see the review by Oudmaijer et al. 2009). Structured circumstellar envelopes of hypergiants formed during several phases of a strong stellar wind with mass-loss rates of 10^{-4}–10^{-3} $M_\odot$ yr^{-1} are sources of IR and maser radiation as well as numerous molecular emission lines. Nevertheless, the yellow hypergiant ρ Cas, nearest to V1302 Aql in the HRD and possessing an extended and unstable atmosphere (Klochkova et al. 2014), shows no signs of circumstellar material (Schuster, Humphreys & Marengo 2006).

Obviously, depending on the adopted nature and hence luminosity of an object, its distance estimate may differ by a factor of a few. However, data obtained during the last two decades from various observations leave no doubts that V1302 Aql is an object at the yellow hypergiant stage (see the review by Oudmaijer et al. (2009) as well as later articles (Driebe et al. 2009; Oudmaijer & de Wit 2013)). Moreover, V1302 Aql is now considered to be the most unambiguous massive Galactic object with high mass-loss rate that undergoes a short-term evolutionary transition from a red supergiant to a Wolf–Rayet star (Meynet & Maeder 2003). One of the most compelling arguments confirming its high-luminosity massive star status has been derived from spectroscopic data obtained at the 6-m telescope of the Russian Academy of Sciences, when Klochkova, Chentsov & Panchuk (1997) found a significant nitrogen excess in the atmosphere of V1302 Aql. In all spectra obtained between 1997 and 2000, a He I λ5876-Å line with a large equivalent width of ≥200 mÅ was detected. With the object's $T_{\rm eff}$ ∼ 9200 K, such an equivalent width could be the consequence of a high luminosity and an enhanced helium abundance in its atmosphere (Miroshnichenko et al. 2013; Klochkova et al. 2002).

Interest in V1302 Aql has been growing in the last decade, due to detection of a 120 K per year $T_{\rm eff}$ increase (Klochkova et al. 1997, 2002; Oudmaijer et al. 1996; Oudmaijer 1998) that allowed researchers to suggest evolution towards the Wolf–Rayet stage. Humphreys, Davidson & Smith (2002) point out that V1302 Aql is a post-red-supergiant star that is crossing a critical HRD region called the Yellow Void (de Jager & Nieuwenhuijzen 1997).

The $T_{\rm eff}$ increase stimulates us to continue spectroscopic monitoring of this mysterious object. High-resolution spectroscopy is required to refine the structure and kinematics of its circumstellar envelope. The most adequate model to represent the observed kinematics is, in our opinion, the 'rain' model proposed by Humphreys et al. (2002) (even taking into consideration the bipolar model suggested later by Oudmaijer & de Wit 2013). Observations with a moderate spectral resolving power, R ∼ 8000, were obtained by Humphreys et al. (2002) to test the model. We obtained spectra with a much higher resolution (up to R ∼ 60 000) that allows us to constrain the line profiles better and to measure their parameters with a much higher accuracy.

In this article, we present the results of a new stage of spectroscopic monitoring of V1302 Aql in a continuation of our study of this object (Klochkova et al. 1997, 2002). In Section 2 we describe our spectroscopic data, Section 3 is devoted to discussion of the results and Section 4 summarizes the conclusions.

2 OBSERVATIONAL DATA

We have added 16 new spectra to our collection of V1302 Aql data from 2001–2014. The observing dates and data spectral ranges are listed in the first two columns of Table 1. Most spectra were obtained with the échelle spectrograph Nasmyth Echelle Spectrograph (NES) (R = 60 000: Panchuk, Yushkin & Najdenov 2003; Panchuk et al. 2009). Our first spectrum, obtained on 2001 August 9, was taken with the spectrograph Lynx (1K×1K CCD, R ∼ 25 000: Panchuk et al. 1993). One-dimensional data were extracted from 2D échelle spectra using the ECHELLE context in Munich Image Data Analysis System, European Southern Observatory (MIDAS), modified to features of the spectrographs used (see details in Yushkin & Klochkova 2005). Cosmic particles were removed by median averaging of two consecutive spectra. Wavelength calibration of the spectra was derived using a Th–Ar hollow cathode lamp.

One of the spectra used in this article was obtained at the McDonald Observatory on 2009 September 11 with the échelle spectrograph TS2 (R = 60 000: Tull et al. 1995) in the coudé focus of

Table 1. Averaged heliocentric velocities for groups of lines in the spectra of V1302 Aql.

Date	Δλ, nm	⟨V$_r$⟩, km s^{-1}						
		Emission		Em./Abs.	Absorption		IS	
		forb.	perm.	Fe II, etc.	Si II+He I	Hα+Hβ	Na I D	DIB
09.08.01	510–670	65	68	36/79	61	68	–	5.6
28.08.04	530–680	67	61	43/83	68	69	11.3	4.8
24.11.07	530–680	65	61	42/77	58	68	11.2	4.5
13.07.08	520–670	65	65	42/79	54	67	11.2	5:
18.08.08	460–600	66	65	45/80	60	70	11.0	5:
3 & 5.11.08	450–590	64	60	46/85	71	72	11.0	4.4
11.09.09	420–880	64	60	39/82	66	69	10.6	3:
31.07.10	440–590	66	59	42/80	60	74	10.8	5:
20.11.10	400–550	64	–	43/80	–	70	–	–
3 & 8.08.12	430–680	65	62	37/81	70	72	10.6	4.4
27.05.13	430–670	64	61	40/81	65	73	10.5	4.8
19.08.13	430–670	66	61	35/80	64	72	10.3	5.2
09.10.13	430–670	66	61	37/82	67	72	10.8	4.6
13.08.14	430–670	66	62	38/83	63	72	11.1	4.2
04.10.14	540–850	65	62	–	65	70	10.5	4:
		Average values of ⟨V$_r$⟩, km s^{-1}						
		65.2 ± 0.3	62.0 ± 0.4	40.5/80.7 ±0.5/0.4	63.7 ±0.3	70.5 ± 0.4	10.8 ± 0.2	4.6 ± 0.2

Notes. Data with reduced accuarcy are marked by colons.

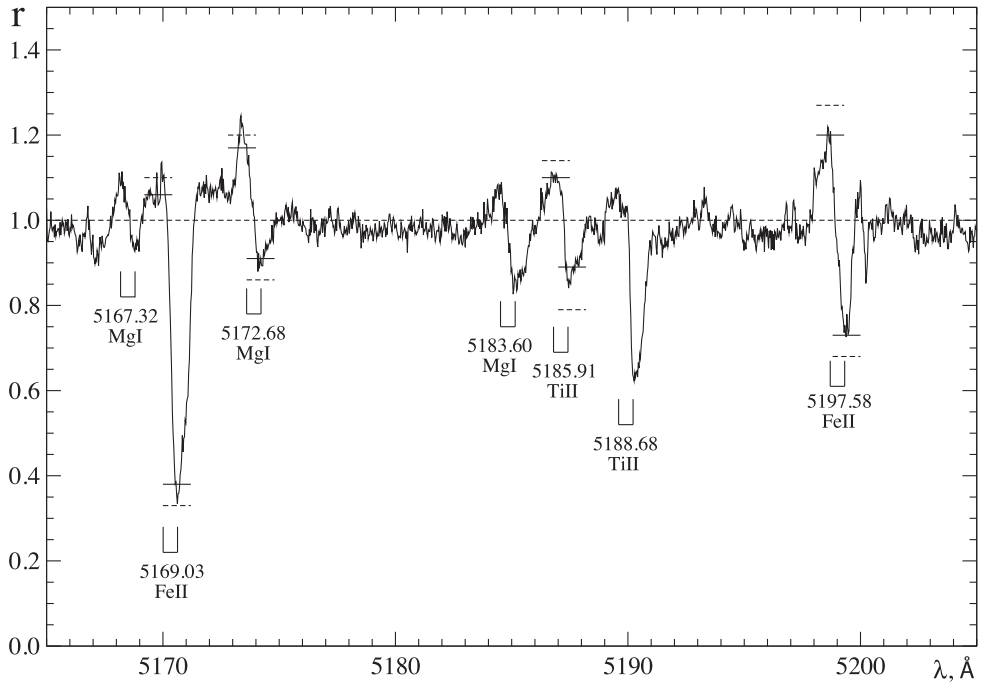

Figure 1. A fragment of the spectrum of V1302 Aql obtained on 2013 August 19 within the region $\Delta\lambda = 5162$–5210 Å. Spectral features with an inverse P Cyg type profile are labelled. Positions of their emission and absorption components are marked by vertical dashes. Short horizontal lines at their peaks indicate the limits of the maximum intensity change registered in 1997 (dashed) and 2001 (solid) compared with the spectrum of 2013.

the 2.7-m Harlan J. Smith telescope. This allowed us to fill the gap in observations with the 6-m telescope for 2009. One-dimensional data for this spectrum were extracted using the *apall* task within the *echelle* package in IRAF. In particular, the spectral range of this observation allowed us to study profiles of the strong lines of Ca II 8408 and 8542 Å in the near-IR region, which is not covered by the 6-m telescope data.

The remaining part of the data reduction, including measurements of the line intensities and positions, was done with the latest version of the DECH20T package (Galazutdinov 1992). This package, traditionally used in our studies, permits radial velocity measurements for individual features of complex line profiles. The procedure of measuring radial velocity is performed by matching the original and mirrored line profiles through shifting of the mirrored profile to a position corresponding to the maximum rank correlation of the original one. Only heliocentric radial velocities, V_r, are used throughout this article. Their systematic errors do not exceed 1 km s^{-1} for a single line. The latter can be seen in the last column of Table 1, where V_r values of the saturated interstellar components of the Na I D lines are listed. Features in the spectrum of V1302 Aql were identified using an atlas by Chentsov, Klochkova & Tavolganskaya (1999) and an atlas by Oudmaijer (1998), which presented a wider spectral interval but with a lower spectral resolution. The standard deviation for pure absorption and emission is $\sigma \leq 0.4$ km s^{-1} and $\sigma = 0.2$ km s^{-1} for the interstellar features.

3 RESULTS AND DISCUSSION

3.1 Spectral type of V1302 Aql in 2001–2014

Earlier spectroscopic observations of V1302 Aql revealed a gradual transition from a normal F-type supergiant (Humphreys et al. 1973) to an A5-type one (Klochkova et al. 2002).

A spectral atlas of this star taken with the CCD échelle spectrograph of the 6-m telescope was published earlier (Chentsov et al. 1999). More than 300 emission features of stellar, circumstellar and interstellar nature have been identified between 4790 and 7520 Å. As an illustration, we present in Fig. 1 a fragment of the spectrum of V1302 Aql within the region $\Delta\lambda = 5162$–5210 Å. The main spectral details that have an inverse P Cyg type profile are identified. The positions of their emission and absorption components are shown by vertical dashes. Short horizontal lines at the peaks of the lines indicate the limits of the maximum change of intensity registered in 1997 (dashed) and 2001 (solid), compared with the spectrum of 2013.

The new spectral type estimates for 2001–2014 based on the same technique presented in Klochkova et al. (1997, 2002) give the following results. Pure absorption lines in the blue part of the spectrum indicate a spectral type A6, while inclusion of criteria using He I and Si II absorption leads to A3.5. Therefore we conclude that the current spectral type coincides with that derived in Klochkova et al. (1997, 2002) within the uncertainties and that the $T_{\rm eff}$ of the object does not grow any further.

3.2 Line profiles in the spectrum of V1302 Aql in 2001–2014

As mentioned earlier, line profiles in the spectra of V1302 Aql vary from purely absorption with small deviations from symmetry to P Cyg type profiles and double-peaked emission. Examples of these line profiles are shown in Fig. 2 in coordinates of the intensity relative to the local continuum, r, versus V_r. Variations of intensities and profiles for the last 20 years (taking into account results from Klochkova et al. 1997, 2002; Humphreys et al. 2002) are noticeable but small. We stress that we cannot expect absolute coincidence of the central velocity of the individual line profiles shown in Fig. 2 and the averaged values of V_r in Table 1, since V_r in Table 1 are averaged

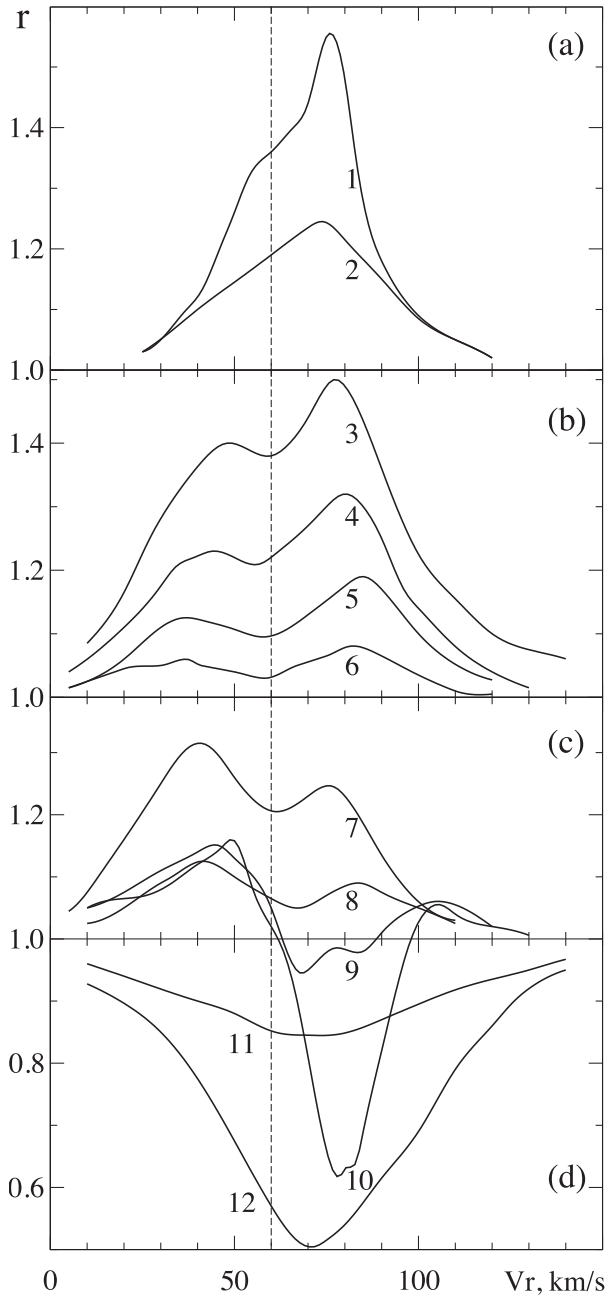

Figure 2. The line-profile transformation in the spectra of V1302 Aql in 2012–2014. The following are shown. Forbidden emission: (1) [Fe II] (Multiplet 14F) 7155 Å; (2) [O I] (1F) 6300 Å. Permitted emission: (3) Fe II (46) 5991; (4) 6084 Å; (5) – 6113 Å; (6) average of Fe I (168) 6394 Å and Ti II (112) 6718 Å; (7) emission Fe II (74) 6417 Å; (8) average of emission Cr II (50) and 5502 Å and 5511 Å. Absorption/emission lines: (9) Ti II (69) 5337 Å; (10) Ti II (70) 5154 Å. Absorption: (11) Si II (5) 5056 Å; (12) Si II (2) 6347 Å. The dashed line shows the systemic velocity $V_{sys} \sim 60$ km s^{-1} (Oudmaijer et al. 1996).

for the sample of numerous lines for every date of observation during 2001–2014. For example, in the spectra obtained on 2012 August 3 and 8, we determined V_r averaged for 7 forbidden emission lines, 26 permitted emission lines, 27 lines with P Cyg type profiles and 15 pure absorption lines.

Hydrogen lines Hα and Hβ in 2001–2014 still have a characteristic double-peaked profile, which was observed in the 1990s (see

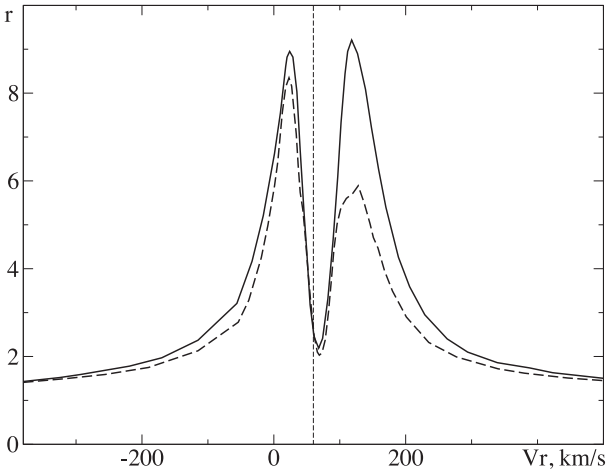

Figure 3. The Hα line profile in the spectra of V1302 Aql in 2007 (solid line) and 2014 (dashed line). The vertical dashed line shows the systemic velocity $V_{sys} \sim 60$ km s^{-1} (Oudmaijer et al. 1996).

fig. 5 in Klochkova et al. 2002). Positions of both emission peaks and the central depression have not changed since then. Variations of the relative intensities of the emission components of both lines remained within 40 per cent. The Hα profiles in two spectra are shown in Fig. 3.

A typical peak intensity ratio for the entire 20-year period of our homogeneous high-resolution observations is seen in the spectrum taken in 2014. A Hα line profile in which the red peak is noticeably higher than the blue one is detected only once, in the spectrum taken on 2007 November 24. In all our other spectra, the peak intensity ratio is the opposite (Klochkova et al. 2002; Humphreys et al. 2002). Such an unusual ratio of intensities of the emission components in Hα for V1302 Aql in the spectrum taken in 2007 is difficult to explain with current models (Driebe et al. 2009; Tiffany et al. 2010; Oudmaijer & de Wit 2013). We suggest that the short-term increase of the red peak in 2007 and the following return to a normal peak intensity ratio may be a short-term appearance of a denser local clump of falling material in a structured envelope. Such a phenomenon may indicate an inhomogeneity of the envelope. Unfortunately, this new phenomenon does not give us an opportunity to choose between the 'rain' (Humphreys et al. 2002) and disc (Oudmaijer & de Wit 2013) models. Variations of the relative intensities of the strongest forbidden and permitted Fe II lines are even weaker (within 10 per cent). Only in the last seven spectra taken in 2012–2014 are they limited to 20 per cent and 6 per cent, respectively.

3.3 Radial velocities of various features in 2001–2014

According to Oudmaijer et al. (1996), the average radial velocity of several rotational bands of the CO molecule with respect to the local standard of rest is V(LSR) = 77 km s^{-1}. The heliocentric systemic radial velocity of the object is $V_{sys} \sim 60$ km s^{-1}. Humphreys et al. (2002) determined $V_{sys} = 58$–60 km s^{-1} using a combination of CO and OH bands. We note that the latter is also close to the velocities derived from radio lines of other molecules (see Quintana-Lacaci et al. 2013, and references therein).

The relative stability of the spectrum of V1302 Aql in recent times and homogeneity of the material obtained allowed us to move from reporting the variety of spectral line shapes to following a gradual transformation between different shapes. Comparison of

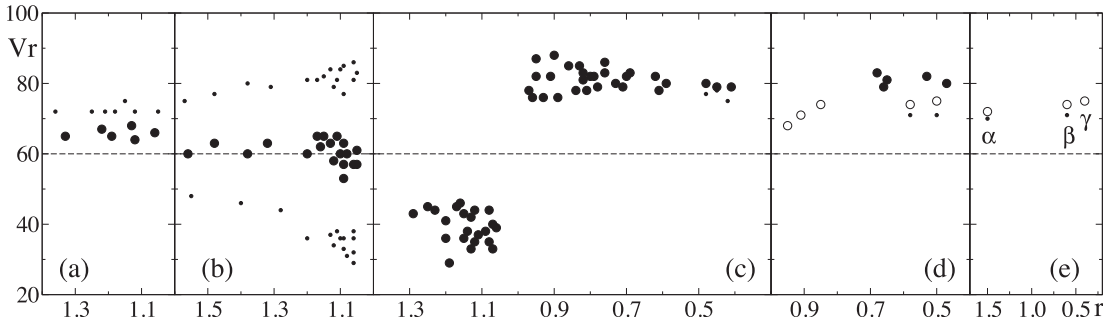

Figure 4. Relationships between the heliocentric radial velocities and relative intensities, r, of the line components in the spectra of V1302 Aql on 2012 August 3 and 8. The horizontal dashed line shows the systemic velocity $V_{sys} \sim 60$ km s^{-1} (Oudmaijer et al. 1996). Here, each symbol denotes one of the components of a line or the dissector of the profile as a whole. (a) Forbidden emission (whole profiles are shown by filled circles, while their peaks are shown by dots). (b) Permitted double-peaked profiles (symbols are the same as in panel (a). (c) Lines with inverse P Cyg profiles (emission and absorption components are shown by filled circles, while cores of the strongest absorption are shown by dots). (d) Fe II absorption (whole profiles are shown by circles) and He I and Si II absorption (whole profiles are shown by open circles, cores are shown by dots). (e) Absorption components of the H I lines (symbols are the same as in panel (d)).

Figs 2 and 4 with the data from Table 1 convinces us that such a transformation is real.

Table 1 shows the averaged values of radial velocities for all spectra. Let us consider the results shown in Table 1 with data for the profiles summarized in Figs 2 and 4. The profiles shown in Fig. 2 are averaged from the spectra taken in 2012–2014. Typical relationships of the radial velocities and relative intensities for emission peaks and absorption cores of individual lines in one spectrum are traced in Fig. 4. The same profile types follow each other from top to bottom in Fig. 2 and from left to right in Fig. 4 and Table 1. Variations of the average radial velocities $\langle V_r \rangle$ of various line groups (see Table 1) are also small. In particular, all radial velocities for pure absorption are in the range $\langle V_r \rangle = 54$–70 km s^{-1}. Forbidden lines are asymmetric (see Fig. 2a): for example, the peak intensity is redshifted with respect to the part of the profile close to continuum, by 6 km s^{-1} on average. The [Ca II](1F) 7291 and 7324 Å emission lines seen in our spectra taken on 2009 September 11 and 2014 October 4 are much stronger that all other forbidden lines, but with no positional shift with respect to the latter. Radial velocities of the entire profiles and their peaks are shown in Fig. 4(a) by circles and dots, respectively. The averaged radial velocities, $\langle V_r \rangle$, measured from the lower parts of the forbidden line profiles are listed in column 3 of Table 1.

As can be seen in Fig. 2, profiles of permitted emission of the iron group are noticeably wider than those for forbidden lines. For example, at approximately equal peak relative intensity near 1.5, their half-widths at the continuum level are 70 and 50 km s^{-1}, respectively. The iron lines are clearly double-peaked, with a weaker blueshifted peak (see Fig. 2b). The radial velocities of the lower parts (close to local continuum) of these emission profiles (in the same way as for the forbidden lines) are shown in column 4 of Table 1 and represented by circles in Fig. 4(b). The emission peak velocities are shown by dots in the same figure. The peak separation decreases from 50 km s^{-1} for weak emission to 26 km s^{-1} for the strongest lines, where it even reaches a triangular shape. It seems that the double-peaked profiles are not simply a sum of two narrower single-peaked emission lines separated by 50 km s^{-1}, but that a partially filled absorption component formed in the stellar atmosphere also takes part in the overall profile formation.

It is seen in Fig. 2(b) and (c) that gradually deepening absorption 'pushes down' the central part of the profile and eventually turns it into an inverse P Cyg type profile. As can be seen from Figs 1 and 2(c), the spectrum contains numerous lines with such profiles, which represent direct evidence of the presence of accretion in the atmosphere of V1302 Aql. For more spectral features, see also the spectral atlas by Chentsov et al. (1999). Line profiles may have this kind of shape in the following cases: when narrow circumstellar absorption overlaps with wide circumstellar emission or when two narrower emission lines with different radial velocities join together. The inner slopes would be shallower than the outer ones in the latter case. We observe steeper inner slopes instead; therefore the emission components are separated by an absorption one. It is possible to have a combination of these two formation mechanisms, as well as the double-ray version suggested in Oudmaijer & de Wit (2013).

There are many lines with emission components on both sides of the absorption in the spectrum of V1302 Aql. We include in the group of lines with inverse P Cyg profiles those with the continuum above the absorption core, $r < 1$. If the central depression is seen at $r > 1$, the line is considered to have a double-peaked profile. Column 5 of Table 1 contains the average radial velocities, $\langle V_r \rangle$, for blueshifted emission and absorption components in the group of lines with P Cyg profiles. Both such components are shown by circles in Fig. 4(c) (an absorption asymmetry is shown for the strongest ones). The redshifted components are weaker ($r < 1.1$) than the blueshifted ones, with an average radial velocity of 130 ± 10 km s^{-1} in our spectra.

The profiles in Fig. 2 differ from classic P Cyg profiles, which represent a spherically symmetric envelope with a radial velocity gradient. The latter show a relationship between the emission component intensity and the absorption component depth. However, in the V1302 Aql spectrum the weakest absorption with $r > 0.95$ may be accompanied by blueshifted emission with any relative intensity in a range $1.0 < r < 1.4$, while the strongest absorption with $r < 0.4$ is seen with the weakest ones ($r < 1.15$). This is seen in Fig. 4, where the leftmost filled circles of the lower chain correspond to the leftmost (not the rightmost!) circles of the upper chain.

Line profiles that are totally located below the continuum make the group of 'absorptions'. However, some of these lines, such as Fe II (37,38), Ti II (31), Cr II, may have hidden outside emission components, because their wings are narrower than those of Si II and Mg II with similar depths. Fig. 4(d) shows the uncertain absorption group members by filled circles, while more reliable ones are shown by open circles. In turn, we consider the most pure absorption components are the weakest ones, such as Si II (4,5) and He I 5876 Å

(the left subgroup of open circles in Fig. 4d). The average radial velocities for the latter lines are given in column 6 of Table 1.

Closeness of the radial velocities seen in Fig. 4 is noticeable in the following line groups.

(i) Iron absorption lines in the blue part of the spectrum and absorption components of the lines with inverse P Cyg profiles (averaging all our data gives $\langle V_r \rangle = 81$ and 80 km s^{-1}, respectively). We consider stable positions of the latter as an indicator of matter infall.

(ii) Strong Si II (2) absorption lines (they are shown by a pair of open circles in Fig. 4d) and absorption components of the Hα and Hβ lines (average radial velocities are $\langle V_r \rangle = 73$ and $\sim$70 km s^{-1}, respectively).

(iii) The weakest absorption and forbidden emission ($\langle V_r \rangle = 63.7$ and 65.2 km s^{-1}, respectively). Since the former forms in the deepest layers of the photosphere (or pseudo-photosphere) while the latter forms in an extended envelope, it is natural that the radial velocity of the latter is only slightly redshifted relative to that of the star's centre of mass, i.e. $V_{sys} \sim 60$ km s^{-1}.

Fig. 4 illustrates all the main features of the kinematic field in the extended atmosphere of V1302 Aql, for observations obtained in 2012 August only. First, we see that even forbidden emission, which originates in the deepest layers of the stellar photosphere (or pseudo-photosphere) and for which we could expect a coincidence with the systemic velocity, is a little ($\sim$5 km s^{-1}) redshifted (Fig. 4a). The permitted emission lines are closer to the systemic velocity and only redshifted by 2 km s^{-1}. Secondly, bisectors of the resolved double-peaked profiles coincide with the systemic velocity (Fig. 4b). Thirdly, the emission peaks and absorption cores of the complex inverse P Cyg profiles are typically located $\sim$40 km s^{-1} apart (Fig. 4c). Fourthly, positions of the cores of the pure strong absorption and absorption components of the hydrogen lines are close to each other (Fig. 4d and e). Finally, positions of the cores of the absorption components of the inverse P Cyg profiles are redshifted by 20 km s^{-1} relative to the systemic velocity. The latter suggests matter infall on to the star.

Some details of the stratified kinematic pattern are already known for V1302 Aql and have been published to some extent in several earlier articles by Oudmaijer (1998), Klochkova et al. (1997, 2002) and Humphreys et al. (2002). However, as can be seen in the data shown in Table 1, all these above-mentioned features are characteristic of every spectrum. Thus, we come to a new and a quite unexpected conclusion for such an unstable star: that we have been observing a constant kinematic state of the atmosphere during 2001–2014. This new result can be considered as additional evidence in favour of the fact that the star has entered a period of slowdown of its evolution.

3.4 Interstellar features in the spectrum of V1302 Aql

Fig. 5 shows a complex profile of the D1 line of a resonance Na I doublet. The main part of its absorption component forms in cold interstellar gas in the line of sight, while a weaker redshifted component forms in the atmosphere of V1302 Aql. The latter is well reproduced by the absorption component of the Fe II 5316-Å line and both can apparently be classified as lines with inverse P Cyg profiles.

The main part of the Na I D line profile in the range $V_r = -25$ to +50 km s^{-1} has an interstellar nature. As follows from a recent compilation of data on the structure and kinematics of the Milky Way (Vallée 2008), the radial velocity in the direction of V1302 Aql

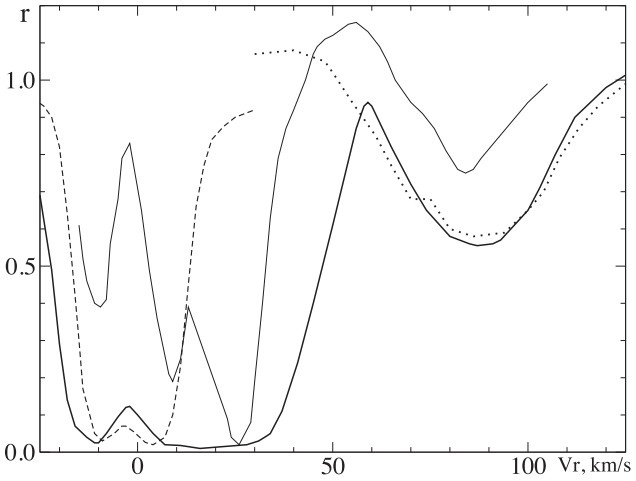

Figure 5. The Na I D1 line profile in the spectra of V1302 Aql (thick solid line) and HD 183143 (dashed line). The thin solid line shows the profile of the K I (1) 7665 Å line in the spectrum of V1302 Aql. The dotted line shows the Fe II 5316 Å line profile in the spectrum of V1302 Aql. Spectra of both stars were taken with the same spectrograph NES. Telluric absorptions and ionospheric emission are removed.

increases with distance and reaches +50 km s^{-1} at a distance $D =$ 5.3 kpc. Fig. 5 shows the Na I D1 line profile in the spectrum of the B-type hypergiant HD 183143, which is projectionally close to V1302 Aql (Galactic coordinates $l/b = 53\overset{\circ}{.}2/0\overset{\circ}{.}6$ and $47\overset{\circ}{.}1/-2\overset{\circ}{.}5$, respectively). However, as seen in fig. 1 of Quintana-Lacaci et al. (2013), HD 183143 is located between the local and Carina–Norma spiral arms, while the line of sight to V1302 Aql passes through the latter arm between 3 and 8 kpc. Therefore, the distance towards HD 183143 is $\sim$2 kpc (Chentsov 2004) and V1302 Aql is located significantly further away. Coincidence of the red boundary of the interstellar Na I absorption and the maximum of the above-mentioned $V_r(D)$ relationship indicates that V1302 Aql cannot be closer than 5.3 kpc. Its spectroscopic parallax moves it even further away, to 6.5–8.0 kpc.

The K I 7665-Å line profile shown in Fig. 5 also represents a combination of stellar and interstellar components. The interstellar components are less saturated compared with those of the Na I D lines and are split into three components. The weakest of them, at $V_r \sim -10$ km s^{-1}, corresponds to the blueshifted component of the Na I D1 line (Fig. 5), while the other two at $V_r \sim 8$ and 24 km s^{-1} are merged in the Na I profile. The stellar absorption component is located at $V_r \sim 84$ km s^{-1}. As clearly seen in Fig. 5, the K I 7665-Å line profile also has an emission component, the position of which at $V_r \sim 56$ km s^{-1} indicates that it forms in the circumstellar envelope.

Using our abundance of high-quality material, we measured the positions of some DIBs. A list of those reliably identifiable in the spectrum of V1302 Aql was published in Chentsov et al. (1999). Note two important points concerning the search and measurement of the DIB positions:

(i) the number of DIBs with measured V_r varies from one spectrum to another (from 5 to 17 features) and
(ii) V_r of the individual DIBs differs systematically.

The latter was mentioned by Oudmaijer (1998), who has identified many DIBs in the object's spectrum. Over 30 of them are narrow and have equivalent widths of $\geq$20 mÅ. The author

explained a large scatter of the measured V_r (from 5–40 km s^{-1}) by uncertain DIB wavelengths.

The last column of Table 1 lists average V_r for each of the observing dates in 2001–2014 of a small group of the narrowest and most symmetric DIBs that show the smallest differential shifts. Their standard wavelengths (5796.97, 5849.82, 6195.96, 6376.00 and 6379.24 Å) are taken from Weselak et al. (2010). After such a selection, the average V_r for all dates came to 4.6 ± 0.2 km s^{-1}. This averaged value is consistent with measurements taken earlier by Oudmaijer (1998) over similar sets of lines, if we consider the difference of the standard wavelengths.

3.5 Closest analogues of the hypergiant V1302 Aql

In Section 1 we mentioned ρ Cas, a well-studied yellow hypergiant with a luminosity similar to that of V1302 Aql. In particular, optical spectra of ρ Cas and the complex structure of its atmosphere and envelope have recently been studied in detail (Gorlova et al. 2006; Klochkova et al. 2014). However, if all features are taken into account, the optical counterpart of the IR source IRAS 18357−0604 turns out to be closer to V1302 Aql. Since this object is very reddened, not many data have been published for it. Recently, Clark, Negueruela & González-Fernández (2014) took a spectrum of IRAS 18357−0604 in the red and IR regions, estimated its distance as $D \sim 6$ kpc using its systemic velocity, classified it as an early A-type star and concluded the similarity of its spectrum to that of V1302 Aql. The spectrum of IRAS 18357−0604 is dominated by asymmetric emission of low-excitation transitions, such as H I, N I, Fe I, Fe II, Ti II, [Fe II], etc. According to Clark et al., the line profile features of IRAS 18357−0604 indicate an asymmetry of its outflowing envelope. However, unlike in the spectrum of V1302 Aql, redshifted components of the broad double-peaked profiles of H I, Ca II and N I in the spectrum of IRAS 18357−0604 are stronger than blueshifted ones.

A bright star HR 8752, the optical counterpart of the IR source IRAS 22579+5640, is also a member of the yellow hypergiants group. It is located much closer to the Sun compared with V1302 Aql and it is easier to study its features. HR 8752 is listed as a standard of Morgan–Keenan (MK) classification, with a spectral type G0 Ia (Morgan & Roman 1950). However, comparing high-resolution spectra taken in 1973–1977, Lambert & Luck (1978) have detected a growth in its $T_{\rm eff}$. The same authors studied the kinematic properties of the star's atmosphere and envelope in detail and noted signs of matter infall on to the star with a speed of 30 km s^{-1}. Later, based on a set of optical spectra of HR 8752 obtained with various instruments in 1973–2005, Nieuwenhuijzen et al. (2012) analysed these data using a homogeneous approach. Adding data from an even longer photometric monitoring, they restored temporal variations of the star's fundamental parameters, such as $T_{\rm eff}$, luminosity, radius, colour index $B - V$, etc. One of their main results is a conclusion regarding the gradual growth of $T_{\rm eff}$ from $\log\ T_{\rm eff} = 3.65$ circa 1900 to $\log\ T_{\rm eff} = 3.90$ in 2000. Therefore, HR 8752 is the closest analogue of V1302 Aql based on all features. At the same time, HR 8752 seems to have a lower mass compared with that of V1302 Aql, judging from the HRD position (Nieuwenhuijzen et al. 2012).

Comparison of the spectral line profiles in our spectra of V1302 Aql in 2001–2014 indicates the absence of noticeable spectral variability, thus allowing us to conclude that this hypergiant entered a phase of slowdown (or termination) of $T_{\rm eff}$ growth and approached the Yellow Void boundary, which is called the White Wall (Oudmaijer & de Wit 2013). Earlier, Patel et al. (2008) suspected stabilization of the star's $T_{\rm eff}$ based on long-term photometric monitoring. New evolutionary loops may follow this episode, such as that observed for HR 8752 on a time-scale of 10 years (de Jager & Nieuwenhuijzen 1997). Therefore, it seems very important to continue monitoring of V1302 Aql.

4 CONCLUSIONS

Using a set of high-resolution spectra of V1302 Aql obtained in 2001–2014, we measured intensities and positions of various spectral features that allowed us to analyse the profile behaviour with time as well as the velocity field in various layers of the object's extended atmosphere and its circumstellar envelope. We concluded on a closeness of V_r for the iron absorption lines in the blue spectral part and absorption components with inverse P Cyg profiles. Positions of the latter features are redshifted by ∼20 km s^{-1}, suggesting that the situation as regards clumps falling on to the star has been stable for all the observing dates.

Hydrogen lines Hα and Hβ in 2001–2014 still have a characteristic double-peaked profile with a stronger blue peak, which was also observed in the 1990s. An Hα profile with the red peak slightly stronger than the blue one was registered in only one spectrum among our collection, which was taken on 2007 November 24. The positions of both emission peaks and the central depression have not changed since then.

The V_r for the weakest absorption components, which form in the deepest observable photospheric (or pseudo-photospheric) layers, and for the forbidden emission, which forms in an extended envelope (63.7 and 65.2 km s^{-1}, respectively). The average V_r of the permitted emission also deviates weakly from that of the pure absorption. It is equal to 62.0 km s^{-1} for all observing dates. On the whole, we have observed a stable kinematic state of the atmosphere during observations in 2001–2014. The average V_r of the DIBs is equal to 4.6 ± 0.2 km s^{-1}.

Comparison of the features in the spectra of V1302 Aql in 2001–2014 indicates the absence of a noticeable variability. We conclude that the hypergiant entered a phase of slowdown (or termination) of $T_{\rm eff}$ growth and approached the high-temperature boundary of the Yellow Void.

ACKNOWLEDGEMENTS

We thank the anonymous referee for valuable suggestions, which helped to improve the quality of the manuscript. This study was accomplished with the financial support of the Russian Foundation for Basic Research (RFBR) in the framework of the project No.14–02–00291a. A.M. acknowledges support for his travel to the McDonald Observatory from the Department of Physics and Astronomy of the University of North Carolina at Greensboro. This research has made use of the SIMBAD database, operated at CDS, Strasbourg, France.

REFERENCES

Blöcker T., 1995, A&A, 299, 755
Chentsov E. L., 2004, Astron. Lett., 30, 325
Chentsov E. L., Klochkova V. G., Tavolganskaya N. S., 1999, Bull. Spec. Astrophys. Obs., 48, 25 (available online at http://arxiv.org/abs/1602.04582)
Clark J. S., Negueruela I., González-Fernández C., 2014, A&A, 561, A15
de Jager C., 1998, ARA&A, 8, 145
de Jager C., Nieuwenhuijzen H., 1997, MNRAS, 290, 50

de Jager C., Lobel A., Nieuwenhuijzen H, Stothers R., 2001, MNRAS, 327, 452
Driebe T. et al., 2009, A&A, 507, 301
Galazutdinov G. A., 1992, Preprint Spec. Astrophys. Obs. No., 92, 1
Gorlova N., Lobel A., Burgasser A. J., Rieke G. H., Ilyin I., Stauffer J. R., 2006, ApJ, 651, 1130
Hrivnak B. J., Kwok S., Volk K. M., 1989, ApJ, 346, 265
Humphreys R. M., Strecker D. W., Murdock T. L., Low F. J., 1973, ApJ, 179, 49
Humphreys R. M., Davidson K., Smith N., 2002, AJ, 124, 1026
Jones T. J., Humphreys R. M., Gehrz R. D., 1993, ApJ, 411, 323
Klochkova V. G., Chentsov E. L., Panchuk V. E., 1997, MNRAS, 292, 19
Klochkova V. G., Yushkin M. V., Chentsov E. L., Panchuk V. E., 2002, Astron. Rep., 46, 139
Klochkova V. G., Panchuk V. E., Tavolganskaya N. S., Usenko I. A., 2014, Astron. Rep., 58, 101
Lambert D. L., Luck R. E., 1978, MNRAS, 184, 405
Meynet G., Maeder A., 2003, A&A, 404, 975
Miroshnichenko A., Danford S., Verdugo E., Klochkova V. G., Chentsov E. L., Zharikov S. V., 2013, in Boumis P., Bonanos A., eds, Massive Stars: From α to Ω. Rhodes, Greece , p. 169
Morgan W. W., Roman N. G., 1950, ApJ, 112, 362
Nieuwenhuijzen H., de Jager C., Kolka I., Israelian G., Lobel A., Zsoldos E., Maeder A., Meynet G., 2012, A&A, 546, A105
Oudmaijer R. D., 1998, A&AS, 129, 541
Oudmaijer R. D., de Wit W.-J., 2013, A&A, 551, A69
Oudmaijer R. D., Groenewegen M. A. T., Matthews H. E., Blommaert J. A. D. L., Sahu K. C., 1996, MNRAS, 280, 1062
Oudmaijer R. D., Davies B., de Wit W.-J., Patel M., 2009, in Luttermoser D. G., Smith B. J., Stencel R. E., eds, ASP Conf. Ser. Vol. 412, The Biggest, Baddest, Coolest Stars. Astron. Soc. Pac., San Francisco, p. 17
Panchuk V. E., Klochkova V. G., Galazutdinov G. A., Ryadchenko V. P., Chentsov E. L., 1993, Astron. Lett., 19, 431
Panchuk V. E., Yushkin M. V., Najdenov I. D., 2003, Preprint Spec. Astrophys. Obs., No. 179, p. 1
Panchuk V. E., Klochkova V. G., Yushkin M. V., Najdenov I. D., 2009, J. Optical Technol., 76, 42
Patel M., Oudmaijer R. D., Vink J. S., Bjorkman J. E., Davies B., Groenewegen M. A. T., Miroshnichenko A. S., Mottam J. C., 2008, MNRAS, 385, 967
Quintana-Lacaci G., Agúndez M., Cernicharo J., Bujarrabal V., Sánchez-Contreras C., Castro-Carrizo A., Alcolea J., 2013, A&A, 560, L2
Schuster M. T., Humphreys R. M., Marengo M., 2006, AJ, 131, 603
Tiffany C., Humphreys R. M., Jones T. J., Davidson K., 2010, AJ, 140, 339
Tull R. G., MacQueen P. J., Sneden C., Lambert D. L., 1995, PASP, 107, 251
Vallée J. P., 2008, AJ, 135, 1301
Weselak T., Galazutdinov G. A., Inwoo H., Krelowski H., 2010, MNRAS, 401, 1308
Yushkin M. V., Klochkova V. G., 2005, Preprint Spec. Astrophys. Obs., No. 206, p. 1

SUPPORTING INFORMATION

Additional Supporting Information may be found in the online version of this article:

suppl_data
(http://www.mnras.oxfordjournals.org/lookup/suppl/doi:10.1093/mnras/stw902/-/DC1).

Please note: Oxford University Press is not responsible for the content or functionality of any supporting materials supplied by the authors. Any queries (other than missing material) should be directed to the corresponding author for the article.

This paper has been typeset from a TEX/LATEX file prepared by the author.